Advances in Aircraft and Spacecraft Science, *Vol. 8, No. 2 (2021) 151-167*
DOI: https://doi.org/10.12989/aas.2021.8.2.151

Stall in ground effect using the unsteady vortex lattice method with Kirchhoff-based correction

Carlos A. Neves[1a] and Pedro J. Boschetti*[2]

[1]*Department of Mechanical Engineering, Universidad Simón Bolívar, Sartenejas Valley, Caracas 1080-A, Venezuela*
[2]*Department of Industrial Technology, Universidad Simón Bolívar, Camuri Valley, Naiguatá 1163, Venezuela*

(Received January 8, 2021, Revised March 22, 2021, Accepted March 24, 2021)

Abstract. The goal of this research is to evaluate the stall behavior of a high aspect ratio rectangular wing in ground effect using an unsteady vortex-lattice method with a Kirchhoff-based correction (UVLM-K), including how the lift coefficient achieved in stall is affected by dynamic ground effect. A flow separation algorithm based on the Kirchhoff-Helmholtz theory and a flow separation model presented by Fischenberg are applied. The code was validated using experimental data from previously published works. The stall behavior of a rectangular wing of aspect ratio of 8.587 formed with a NACA 4415 airfoil section was studied in static and dynamic ground effect. To obtain the empirical data required by the UVLM-K, the NACA4415 airfoil was simulated at fixed height aboveground using a finite-volume code solver. The wing simulation results have shown that the lift coefficient achieved by the wing in stall for takeoff and flare maneuvers are lower than those estimated at a fixed height above the ground. It can be concluded, based on the results obtained herein, that the stall behavior of a wing in dynamic ground effect depends on the history of the maneuver.

Keywords: unsteady aerodynamics; stall prediction; ground effect; computational fluid dynamics; take-off and landing; Kirchhoff flow theory

1. Introduction

During takeoff and landing, airplanes fly at a height above the ground that is relatively small compared to their dimensions, and their aerodynamic characteristics change with respect to those in free flight. This phenomenon is known as the ground effect (Nuhait and Mook 1989, Staufenbiel and Schlichting 1988). Additionally, during these maneuvers, aircraft are operating at high lift coefficients and angles of attack, which are the most hazardous flight conditions (Syms 2002). In fact, between 2009 and 2018, 49% of fatal accidents in the commercial jet airplane fleet worldwide occurred during final approach and landing, and 12% occurred during takeoff and initial climb (Boeing 2019).

Variations in the aerodynamic characteristics of wings and airplanes due to ground proximity have been widely studied. Data obtained via wind tunnel testing on rectangular wings of aspect ratio (R_A) equal to 3.46 and 5.18 at fixed height aboveground show an increase in lift, a significant

*Corresponding author, Associate Professor, E-mail: pboschetti@usb.ve
[a]Undergraduate Student, E-mail: carlosneves37@gmail.com

Copyright © 2021 Techno-Press, Ltd.
http://www.techno-press.org/?journal=aas&subpage=7 ISSN: 2287-528X (Print), 2287-5271 (Online)

reduction in induced drag, and a systematic increase in viscous drag in ground effect with respect to free flight data (Traub, 2015). Moreover, when the ground height is a function of time, the aerodynamic forces and moments are time-variant, resulting in an unsteady flow phenomenon known as the unsteady or dynamic ground effect (Chen and Schweikhard 1985). Chen and Schweikhard (1985) simulated a two-dimensional flat plate at low angles of attack in sink maneuvers using a quasi-vortex-lattice method, and differences were found between lift coefficient values achieved in static ground effect and those calculated in dynamic ground effect. Cambered wings were simulated using an unsteady vortex-lattice method (UVLM), in descent maneuvers and the results showed that changes in aerodynamic coefficients increase with proximity to the ground (Nuhait, 1995). Simulations performed by a vortex-ring panel code on a rectangular wing of high aspect ratio at a constant sink rate and in flare maneuver demonstrated that the sink rate produces significant variations in aerodynamic coefficients of a wing (Boschetti *et al.* 2016, 2017, Quijada and Boschetti 2015). Using an unsteady vortex-lattice code, it was demonstrated that the lift, induced drag, and pitching moment coefficients are linked to a specific history of the flight path or trajectory of a wing or airplane in ground effect (Boschetti *et al.* 2020m Merkl *et al.*2019).

The maximum lift coefficient ($C_{L,max}$) for airplanes or wings in ground effect can be reduced with respect to out of ground effect condition, a fact that might not be recognized industry-wide (National Transportation Safety Board, 2012). Computational fluid dynamics (CFD) codes based on Reynolds-averaged Navier-Stokes and lattice Boltzmann method can predict the lift coefficient reasonably well for a representative transport airplane in high lift configuration (Rumsey *et al.* 2011, 2015, 2019). However, the CPU time and overhead in memory using these codes can be in some cases prohibitive (Leishman and Beddoes, 1989).

Some computational methods can estimate the maximum lift coefficient by knowing the inviscid flow field of a three-dimensional configuration, employing a two-dimensional flow criterion, assuming that viscous effects are generally locally two-dimensional (Sym, 2002), with a relatively low computational cost. Leishman and Beddoes used an indicial response and superposition method combined with the Kirchhoff theory to model the nonlinear effects of trailing edge separation on an airfoil employing empirical flow separation data. This method was able to model accurately the dynamic stall of the airfoil studied (Leishman and Beddoes 1989). Fischenberg (1995) carried out a similar analysis on a six-degrees-of-freedom aircraft simulator and satisfactory post-stall results were obtained. Dynamic wind tunnel and flight test data from highly maneuverable aircraft demonstrated the lift dependency on the angle of attack and pitch rate at high angles of attack, therefore, high-quality aerodynamic models for unsteady effects including flow separation are encouraged to increase the fidelity in the high lift and stall region (Fischenberg 1995). Dias (2016) proposed a nonlinear lifting-line algorithm combined with the Kirchhoff theory to assess the post-stall conditions and unsteady aerodynamic hysteresis effects in a group of wings. A similar nonlinear methodology based on a steady vortex-lattice method (VLM) was developed obtaining results in very close agreement with values achieved by wind tunnel testing and nonlinear CFD (dos Santos and Marques 2018).

The objective of this research is to evaluate the stall behavior of a high aspect ratio rectangular wing in ground effect using an unsteady vortex-lattice method with a Kirchhoff-based correction, including how the lift coefficient achieved in stall is affected by dynamic ground effect. A better understanding of the stall phenomenon in ground effect can guide future studies and analyses in this area, moreover, they may help to improve the aerodynamic models of airplanes, which are required for flight dynamics simulation.

2. Method

2.1 Unsteady vortex-lattice method

The code built for the fluid dynamics analysis used herein is based on the UVLM. This time-domain method aims to obtain the strength of the vortex-ring elements in the mesh surface using an extension of the VLM to non-stationary situations (Murua *et al.* 2012). Hence, this can solve unsteady, incompressible, and inviscid fluid flow around a three-dimensional configuration. The code is based on the theory presented by Katz and Plotkin (2001). Ground effect is modeled by the image method (Katz and Plotkin 2001), and a wake relaxation scheme is used for the wake rollup in the Trefftz plane. The vortex strengths ($\mathbf{\Gamma}_t$) are computed through Eq. (1), which solves the Laplace equation by complying with the flow tangency and Kutta condition,

$$\begin{bmatrix} a_{11} & \cdots & a_{1L} \\ \vdots & \ddots & \vdots \\ a_{K1} & \cdots & a_{KL} \end{bmatrix}_t \begin{bmatrix} \Gamma_1 \\ \vdots \\ \Gamma_K \end{bmatrix}_t = \begin{bmatrix} RHS_1 \\ \vdots \\ RHS_K \end{bmatrix}_t \tag{1}$$

where the a terms correspond to the influence coefficients, which are obtained by evaluating the induced velocity of the L vortex rings at each K collocation point on the wing surface without thickness, and the ***RHS*** vector corresponds to the induced velocity of the known singularities in the space at each collocation point K (Katz and Plotkin 2001). However, to generate appropriate results, the singular conditions of the vortices ought to be addressed. The technique chosen in the present work to modify the singular behavior of the vortex filaments corresponds to a cut-off scheme of the Biot-Savart law shown in Eq. (2) (Sarpkaya 1989). This scheme uses a vortex core radius (δ_c<<1) to smooth the velocity profile near the vicinity of the vortex filaments, and hence avoids singular conditions in the solution.

$$\mathbf{V}_\Gamma = \frac{\Gamma}{4\pi} \frac{\mathbf{r}_1 \times \mathbf{r}_2}{\left| \left(\mathbf{r}_1 \times \mathbf{r}_2\right) + \left(\delta_c \left|\mathbf{r}_o\right|\right)^2 \right|^2} \mathrm{r}_o \left(\frac{\mathbf{r}_1}{\left|\mathbf{r}_1\right| + \delta_c \left|\mathbf{r}_o\right|} - \frac{\mathbf{r}_2}{\left|\mathbf{r}_2\right| + \delta_c \left|\mathbf{r}_o\right|} \right) \tag{2}$$

where $\mathbf{r_o}$ is the vortex line vector, and $\mathbf{r_1}$ and $\mathbf{r_2}$ are the points 1 and 2 of the Biot-Savart law, respectively.

2.2 Kirchhoff-based correction

Due to the inviscid characteristics of the resultant flow field obtained using the UVLM, the method becomes unsuitable for aerodynamic analyses at high angles of attack. To take into account the nonlinearities produced by flow separation, a correction must be embedded in the UVLM to model the wing stall and post-stall behavior, such as the Kirchhoff-Helmholtz theory (dos Santos and Marques 2018).

The Kirchhoff-Helmholtz correction, originally developed for steady flow analyses, corrects the lift coefficient of an airfoil (C_l) by the amount of flow separation f on its extrados at a given angle of attack (α) as (dos Santos and Marques 2018),

$$C_l = C_{l\alpha} \left(\frac{1+\sqrt{f}}{2} \right)^2 \alpha \tag{3}$$

The model used in this research to estimate the flow separation parameter f was presented by Fischenberg (1995) and applied by Dias (2016),

$$f = \frac{1}{2}\left\{1 - \tanh\left[a_1\left(\alpha - \alpha^* - \tau_2\dot{\alpha}\right)\right]\right\} \tag{4}$$

The term a_1 represents the stall abruptness of the airfoil, and α^* is the angle of attack corresponding to f=0.5, and τ_2 is a parameter used to account for dynamic flow separation and reattachment hysteresis. Both terms, a_1 and α^*, are obtained from experiments or CFD simulations in the steady fluid flow (Dias 2016, Fischenberg 1995). Additional details about this phenomenon can be found in Fischenberg (1995) and Leishman and Beddoes (1989).

2.3 Kirchhoff-based correction of the unsteady vortex-lattice method

In the steady VLM, it is sought to apply the nonlinear correction to the vortex ring strengths, so as to correct the influence coefficients. Considering that the wing is divided into spanwise sections, the effective angle of attack of the N^{th} spanwise section yields to a local flow separation f_N, hence the influence coefficients that reside in the mentioned section are corrected as follows (dos Santos and Marques 2018).

$$a_{K,L}{}^{*} = \frac{4a_{K,L}}{\left(1+\sqrt{f_N}\right)^2} \tag{5}$$

Since the Kirchhoff-based correction is a methodology developed to the steady solution of the Laplace equation, the correction algorithm cannot be activated until a steady solution is obtained (Dias 2016). Furthermore, when ground effect is considered, the empirical constants of the flow separation modeled in Eq. (4) may vary with height since the ground plane affects the stall behavior of an airfoil (Lee *et al*. 2018, Traub 2015). Therefore, when the Kirchhoff-based correction algorithm is used in ground effect, a database containing the airfoil α* and a_1 coefficients at different heights is required. These coefficients are hereinafter referred to as "stall parameters".

After a UVLM inviscid solution is attained in steady flow, the Kirchhoff-based correction algorithm is activated under the following iterative procedure:

• Computation of the coefficients of the flow separation model f at the current height at each wingspan section.

• Computation of the flow separation distribution with Eq. (4) using the effective angle of attack distribution along the wingspan.

• Correction of the influence coefficients by Eq. (5) with the flow separation distribution obtained in step 2.

• Repetition of the UVLM routine at the current time step with the corrected influence coefficient matrix to generate a new set of corrected vortex strengths $\mathbf{\Gamma}_t$.

• The correction cycle is repeated since the new distribution of effective angles of attack is produced in step 4. The iterations stop once a convergence criterion is attained. The convergence criterion used is the maximum separation flow error along the wingspan (Dias 2016, dos Santos & Marques 2018).

This numerical procedure tends to be unstable when a large number of iterations before convergence is achieved. Although these instabilities do not affect the results of the lift coefficient

(Dias, 2016), they are undesirable in the UVLM because they are propagated towards the wake. To mitigate the instabilities, a damping factor $DF \in (0,1]$ is used to correct the results of f obtained at each iteration, and the flow separation at a given N^{th} section is only updated if the local lift coefficient is reduced in comparison with the previous iteration (Dias 2016).

$$f_{N,it} = DF \cdot f_{N,it} + (1 - DF)\, f_{N,it-1} \tag{6}$$

In the present research, the correction algorithm is activated at the time interval in which the steady and inviscid solution is obtained and in following intervals where a change in angle of attack and/or height occurs. Henceforth, the influence coefficient matrix becomes a function of height and the angle of attack. Changes in the angle of attack and height are executed by the code once the corrected aerodynamic coefficients achieve a steady-state in steady flight.

3. Results and discussion

3.1 Validation of the method

To validate the capabilities of the UVLM code with a Kirchhoff-based correction (UVLM-K) to estimate stall behavior in ground effect, a rectangular and untwisted wing of R_A=5.18, and a geometric mean chord (c) of 0.1016 m formed with an S8036 airfoil section was simulated at Re=1.20×10^5. These results are compared with the experimental values obtained via wind tunnel testing by Traub (2015). The modeled wing has 16 chordwise and 50 spanwise divisions. Differences of less than 0.1 % were reached between the values of the aerodynamic coefficients attained for different panel distributions. Likewise, in free flight using a time step of 0.5 s, the inviscid aerodynamic coefficients achieved at α=14 deg do not change excessively after 2 s, and they reached a steady condition at 6.5 s. The Kirchhoff correction was activated at 7.5 s, and the viscous aerodynamic coefficients reached a steady condition at 9 s. In this paper, the convergence criterion employed for f in the Kirchhoff-based correction is 0.005 and a DF of 0.1 is used.

The airfoil stall parameters required for the simulations were calculated at different heights using Eq. (3) and the data presented by Traub (2015). Table 1 shows these coefficients as a function of the nondimensional height (h=H/c) for this airfoil.

Fig. 1 illustrates the lift coefficient as a function of angle of attack at different heights estimated by the UVLM-K compared with the experimental data by Traub (2015). These values are shown along with those obtained using a steady VLM with a Kirchhoff-based correction (VLM-K). It can be observed that the values of the maximum lift coefficient estimated by the UVLM-K code are in good correlation with respect to those obtained by wind tunnel testing for height-to-span (H/b)

Table 1 Stall parameters of the S8036 airfoils at Re=1.2×10^5 at different heights

h	α^*, deg	a_1, deg^{-1}
∞	14.76	0.4652
1.0	14.68	0.4555
0.8	14.49	0.4014
0.6	14.36	0.3638
0.4	13.58	0.2612

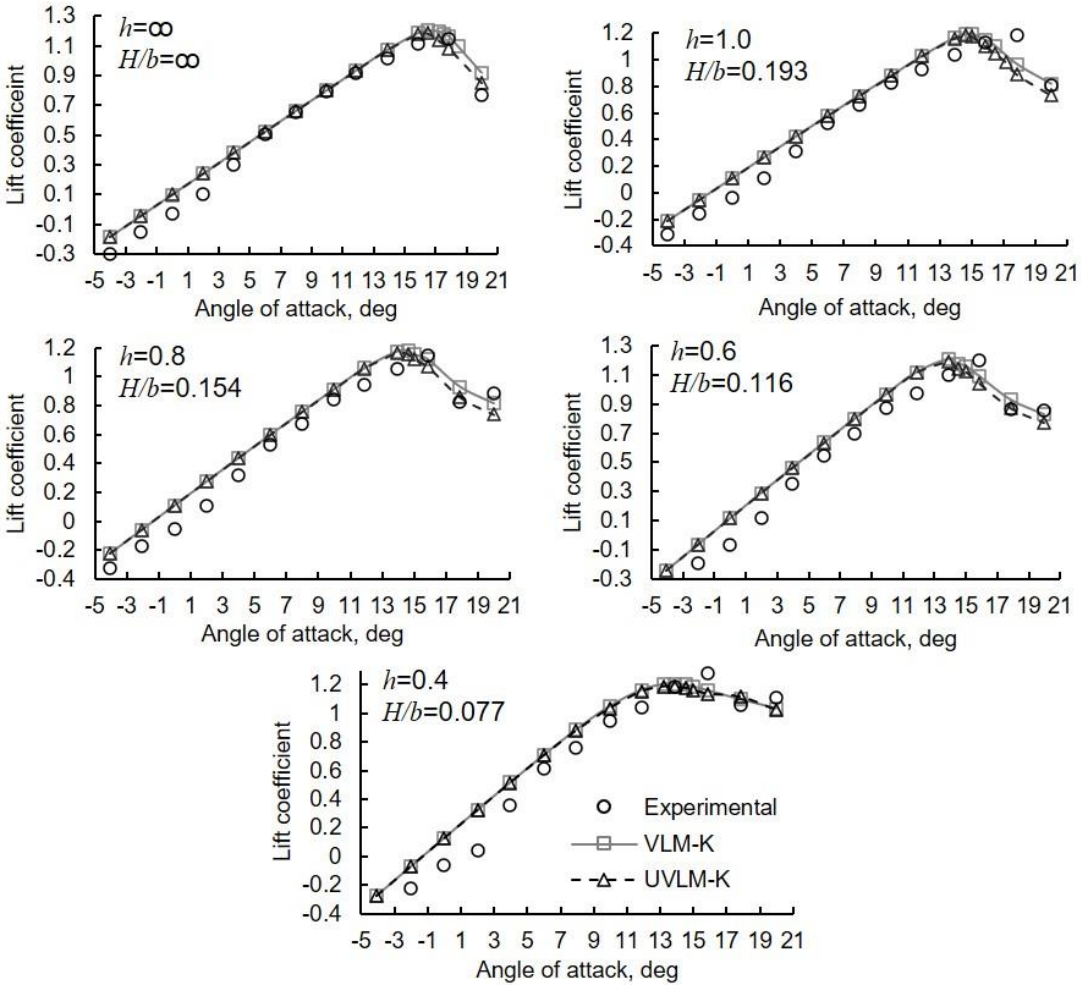

Fig. 1 Lift coefficient as a function of angle of attack at different heights in static ground effect

greater or equal to 0.116 with a maximum difference of 3.05% in free flight, while the error achieved at *H/b*=0.077 is 7.93%. The stall onset was satisfactorily modeled for the wing studied. These numerical methods acceptably predicted the post-stall behavior of the wing for *H/b* equal to ∞, 0.154, and 0.116. Additionally, at small angles of attack, the difference with respect to experimental values of C_L increases as height decreases.

It is seen in Fig. 1 that at high angles of attack, the lift coefficients computed with the UVLM-K are slightly lower than those obtained with the VLM-K. The reason for the difference between the results of both methods is that when the UVLM-K is used, at the time intervals in which the Kirchhoff-correction algorithm is activated, the wing sheds corrected-circulation vortex rings, thus developing a corrected-flow wake while the corrected aerodynamic coefficients achieve a new steady state. This corrected-flow wake development in time is not accounted for in the VLM-K where the Kirchhoff correction is done to a single-interval inviscid steady flow solution.

Fig. 2 shows the evolution in time of the lift coefficient in free flight at steady condition for the wing studied at angles of attack of 8, 14, and 18 deg using the UVLM-K with the Kirchhoff

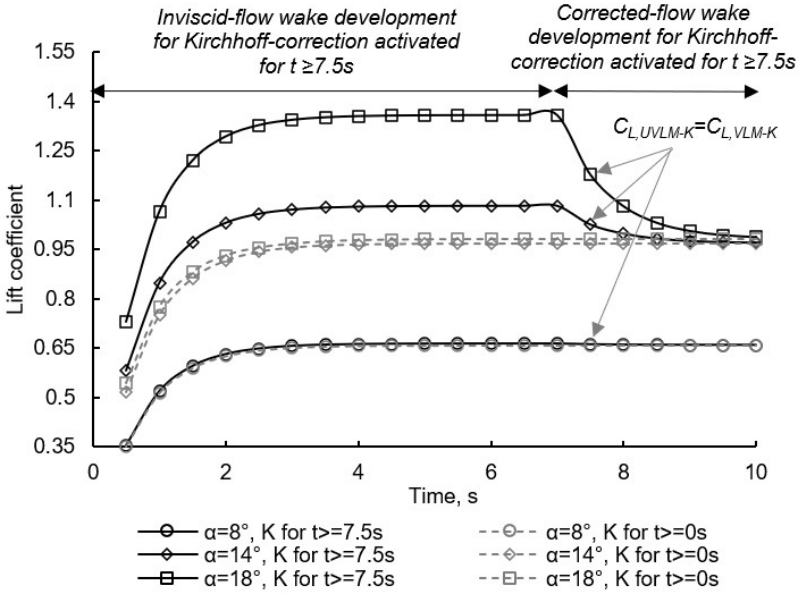

Fig. 2 Evolution in time of the lift coefficient using the UVLM-K

correction activated once the aerodynamic coefficients achieve a steady state. At t = 7.5 s it is seen a sudden drop of lift for α equal to 14 and 18 deg, due to the activation of the Kirchhoff correction at this time interval, resulting in the same value as the one obtained using the VLM-K. However, the Kirchhoff correction generates a new matrix of corrected influence coefficients for $t \geq 7.5$ s and as the wing continues to advance, the corrected lift coefficient decreases until it achieves a new steady state. No changes are observed for α = 8 deg since the correction is negligible. Additionally, if a different methodology is considered in which the Kirchhoff-correction is activated for $t \geq 0$ s, the lift coefficient achieves a steady-state whose value differs less than 0.5% with respect to those attained with the Kirchhoff correction activated once the inviscid solution is achieved. Using the Kirchhoff correction for $t \geq 0$ s is not considered in this paper since the Kirchhoff flow correction is theoretically based on correcting an inviscid steady flow solution.

3.2 Stall in dynamic ground effect

The study of the stall behavior of a wing of R_A=8.587 and c=0.604 m formed with a NACA 4415 airfoil section is presented in flare and takeoff maneuvers in dynamic ground effect. Also, analyses of the vortex strength distribution on the wake developed in the simulations are presented to assess the influence of ground effect and the point of flow separation distribution computed by the Kirchhoff correction on its shape and wing stall. This wing was previously studied in inviscid flow in static ground effect through high order panel code (Boschetti *et al.* 2010), and in static and dynamic ground effect by a previous version of the code used herein (Boschetti *et al.* 2016, 2017, 2020, Merkl *et al.* 2019, Quijada and Boschetti 2015).

To obtain the stall parameters of the NACA 4415 airfoil, the aerodynamic data obtained using the double-precision solver of ANSYS FLUENT 19.2 ACADEMIC at M_∞=0.09364, and Re=1.2×10^6 shown by Páez Castro (2019) was employed. Table 2 shows the stall parameters of the NACA 4415 airfoil at different heights aboveground.

Table 2 Stall parameters of the NACA 4415 airfoil in free flight and in ground effect at Re=1.2×10^6

h	α*, deg	a_1, deg^{-1}
∞	17.0175	0.176837
2.424	17.21	0.148657
1.759	16.9605	0.153259
1.278	16.343	0.175732
0.8	16.3169	0.164939

Table 3 Aerodynamic parameters of the wing at different heights

h	H/b	$C_{L\alpha}$, rad^{-1}	C_{L0}	$C_{L,max}$
∞	∞	4.5836	0.3385	1.3858
8.7251	1.0160	4.5893	0.3392	1.3606
6.3162	0.7355	4.6008	0.3403	1.3556
4.5875	0.5342	4.6123	0.3422	1.3470
3.3311	0.3879	4.6409	0.3450	1.3429
2.4241	0.2823	4.6982	0.3491	1.3311
1.7599	0.2049	4.7670	0.3544	1.3136
1.2778	0.1488	4.8987	0.3616	1.3038
0.8000	0.0932	5.0878	0.3747	1.3091

3.2.1 Static stall of a rectangular wing in static ground effect

The aforementioned wing of R_A=8.587 was simulated by the UVLM-K moving at different fixed heights above the ground in subsonic incompressible flow at Re=1.20×10^6. The stall parameters for the NACA 4415 airfoil are contained in Table 2. The wing simulated has 26 chordwise and 56 spanwise divisions. Differences of less than 0.003 % were reached between the values of the aerodynamic coefficients attained for different panel distributions. Similarly, the aerodynamic coefficients achieved at α=14 deg in free flight using a time step of 0.5 s do not change excessively after 4 s and they reached a steady condition at 6.5 s. Afterward, at the same angle of attack, the Kirchhoff-correction was activated at 7.5 s and the corrected aerodynamic coefficients achieved a steady condition at 10 s.

Table 3 presents the aerodynamic performance of the wing obtained at different heights aboveground. As height diminishes, there is a decrease of maximum lift coefficient, and an increase of lift slope ($C_{L\alpha}$) and lift coefficient at zero angle of attack (C_{L0}).

As an addition to the study of the stall in static ground effect, Fig. 3 illustrates the wakes generated by the wing at α=17 deg in free flight (in stall) and in ground effect (in post-stall) at a fixed height aboveground. The purpose of studying the wake in this work comes after the dependence of the wake induced velocity, which is used for the computations of the ***RHS*** vector and the induced drag coefficient related to the effective angle of attack distribution along the wingspan at each time interval, on the development of the wake shape (Katz & Plotkin, 2001). The latter is influenced by the Kirchhoff-correction methodology employed and ground proximity. Moreover, the wake shape is a direct result of the vortex strength distribution on the wing since vortices are produced at wingspan sections with weaker vortex strength, thus allowing the assessment of the Kirchhoff correction along the wingspan.

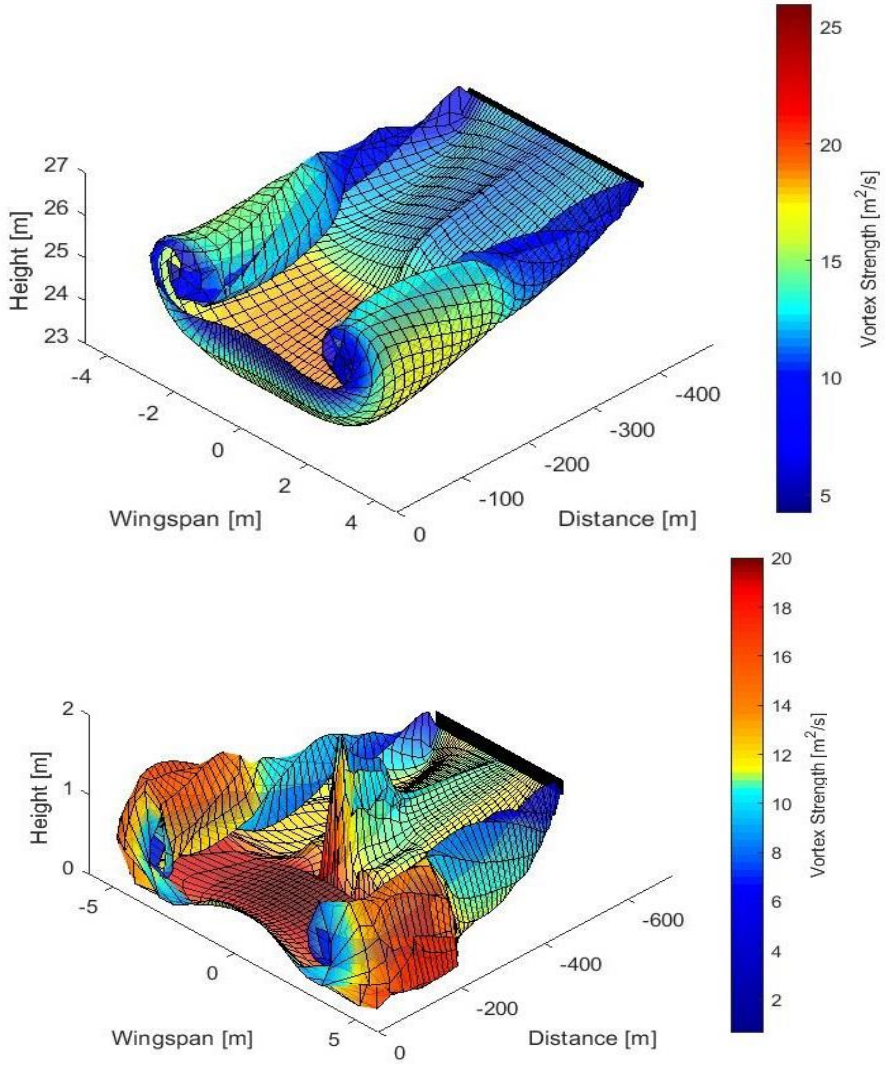

Fig. 3 Wakes generated in free flight (top) and at H/b=0.1488 (bottom) both at α=17 deg

The main differences between the two wakes shown in Fig. 3 can be seen at the wing root and wingtips. In unbounded flow field, the wingtip vortices are fully developed whereas in ground effect the wake at the wingtip vortices is flattened and widened. Furthermore, in unbounded flow field, the wake along the wingspan has a downward displacement due to the roll-up while in ground effect the downward displacement of the wake is limited by the ground plane.

For both wakes presented in Fig. 3, the corrected-flow wake can be distinguished from the inviscid-flow wake by identifying the presence of a peak on the wing root vicinity of the corrected-flow wake and the sudden change of vortex-strength distribution. The peak in the corrected-flow wake on the wing root vicinity is produced because its vortex rings have lower strength, hence they are heaved by the induced velocity of greater-strength vortex rings next to them. The strength of the wake vortex rings on the wing root vicinity is lower than others near to

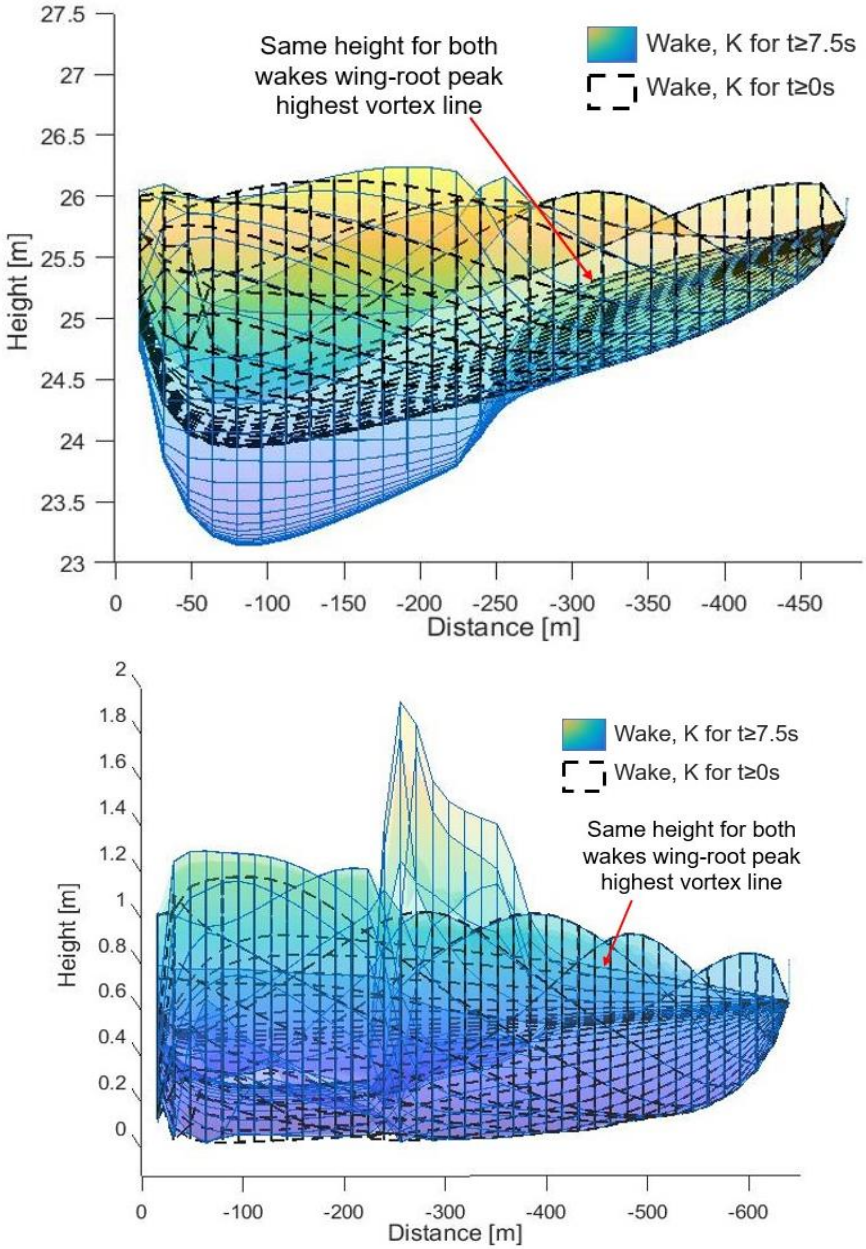

Fig. 4 Wakes generated with the Kirchhoff correction activated for $t \geq 7.5$ s and $t \geq 0$ s in free flight (top) and at H/b=0.1488 (bottom) both at α=17 deg

them along the wingspan because the point of flow separation on the wing has lower values at the wing root, thus resulting in greater corrections to the influence coefficients for wingspan sections on the wing root vicinity (i.e., a lower value for the point of flow separation produces a greater vortex strength correction at a given wingspan section as per Eq. (5)).

By comparing both wakes shown in Fig. 3, it is observed that the peak at the wing root vicinity of the corrected-flow wake is less pronounced in unbounded flow field than in ground effect. This occurs because the point of flow separation values are lower in ground effect than in unbounded flow field for the studied wing at the same angle of attack, therefore the reduction of maximum angle of attack in static ground effect as the wing decreases its height.

An additional concern arises from the interaction between the inviscid-flow wake and the corrected-flow wake on the aerodynamic coefficient evolution in time and the resultant wake shape since the Kirchhoff-correction is activated at t=7.5 s. In ground effect simulation of Fig. 3, it is seen that abrupt upward displacements are produced on the corrected-flow wake vortex rings shed near to t=7.5 s (i.e., Kirchhoff-correction activation) on the wing root vicinity. However, it is also observed that the corrected-flow wake development is stabilized once its vortex rings are shed in the inviscid-flow wake far field. It can be considered that the strong interaction between the inviscid-flow and the corrected-flow wakes at the time intervals near to t=7.5 s may affect the history-sensible, aerodynamic analysis. Nonetheless, the corrected-flow wake developed in the far-field of the inviscid-flow wake has negligible differences with respect to a wake developed using the Kirchhoff correction since t=0 s, as carefully observed in Fig. 4. Thus, the methodology employed for the activation of the Kirchhoff correction once the inviscid steady flow is established becomes suitable for the aerodynamic analysis given the study of Figs. 2 and 4. The colormap of Fig. 4 is related to the height of the vortex rings.

3.2.2 Stall of a rectangular wing in dynamic ground effect

The wing is simulated in flare and takeoff maneuvers to evaluate the stall behavior in dynamic ground effect. These simulations were carried out with an initial velocity of 32.02 m/s, and at a ground distance of 300 m. Before starting each maneuver, the wing flies at an initial fixed height aboveground at an initial angle of attack (α_o) until the aerodynamic coefficients calculated using the Kirchhoff-based correction acquired a steady condition and the corrected-flow wake develops on the far-field of the inviscid-flow wake; then, the wing performs the corresponding flare or takeoff maneuver, followed with a flight at a fixed height aboveground until a steady condition is achieved. For flare maneuvers, the initial height-to-span ratio is equal to 1.016, and the final H/b is 0.1488, and for takeoff, the initial H/b is 0.1488, and the final H/b is 1.016. Flare and takeoff maneuvers are modeled employing the expression established by Blakelock (1991) shown in Eq. (7), where H_0 is the highest height and τ can be estimated by the distance to the touchdown point, knowing that the sink (or climb) rate $\dot{H}$ is equal to $-H/\tau$.

$$H = H_0 \cdot e^{-t/\tau} \tag{7}$$

For these maneuvers, the pitch angle (θ) changes as a function of time. In this paper, two different models for the pitch angle variation are used. Eqs. (8) and (9) correspond to a constant and an exponential rate of change of pitch angle, which are linked to M_θ and K_θ, respectively. These equations employ the flight-path angle at the beginning (γ_1) and the end (γ_2) of the maneuver, for takeoff, $\theta_1=\gamma_1$ and $\theta_2=\gamma_2$, and flare $\theta_1=\gamma_2$ and $\theta_2=\gamma_1$.

$$\theta(t) = M_\theta\left[t(\theta_2-\theta_1)/(t_2-t_1)+\theta_1\right] \tag{8}$$

$$\theta(t) = K_\theta\theta_2 e^{\frac{t_2-t}{\tau_\theta}}; \quad \tau_\theta = (t_2-t_1)/\ln(K_\theta\theta_2/\theta_1) \tag{9}$$

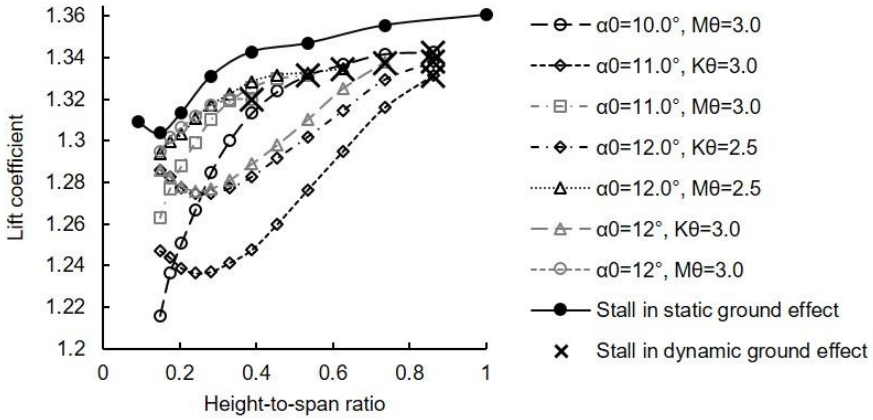

Fig. 5 Stall in dynamic ground effect in takeoff maneuver

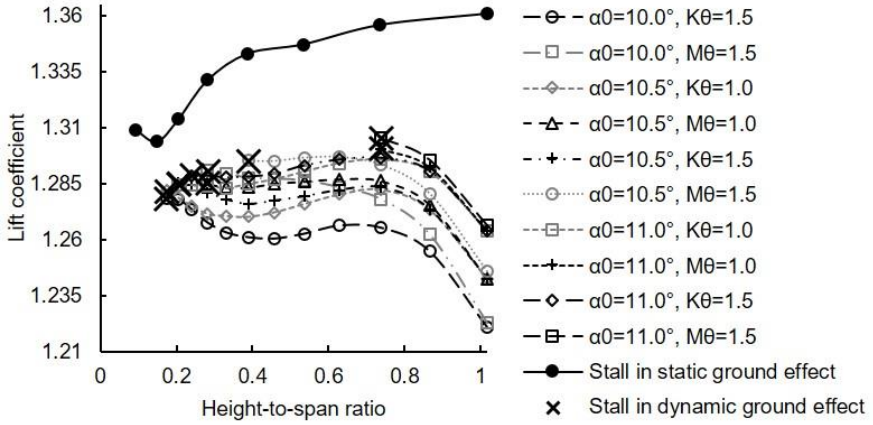

Fig. 6 Stall in dynamic ground effect in flare maneuver

Table 4 Lift coefficient achieved by the wing in stall for the take-off maneuvers simulated

α_0, degrees	K_θ	M_θ	C_L	H/b
10.00	-	3.0	1.3427	0.8619
11.00	3.0	-	1.3315	0.8619
11.00	-	3.0	1.3318	0.5338
12.00	2.5	-	1.3381	0.8624
12.00	-	2.5	1.3345	0.6265
12.00	3.0	-	1.3379	0.7347
12.00	-	3.0	1.3201	0.3878

The values for K_θ and M_θ used in the simulations were chosen to achieve the stall during the maneuvers, while the product $\tau_2\dot{\alpha}$ in Eq. (4) is negligible. The simulations were performed at a time step of 0.5 s since negligible changes were observed with respect to the results obtained using smaller time steps.

Table 5 Lift coefficient achieved by the wing in stall for the flare maneuvers simulated

α_o, degrees	K_θ	M_θ	C_L	H/b
10.00	1.5	-	1.2784	0.1744
10.00	-	1.5	1.2908	0.2822
10.50	1.0	-	1.2819	0.1744
10.50	-	1.0	1.2849	0.2822
10.50	1.5	-	1.2852	0.2048
10.50	-	1.5	1.2951	0.3888
11.00	1.0	-	1.2846	0.2048
11.00	-	1.0	1.3005	0.7376
11.00	1.5	-	1.2885	0.2404
11.00	-	1.5	1.3052	0.7376

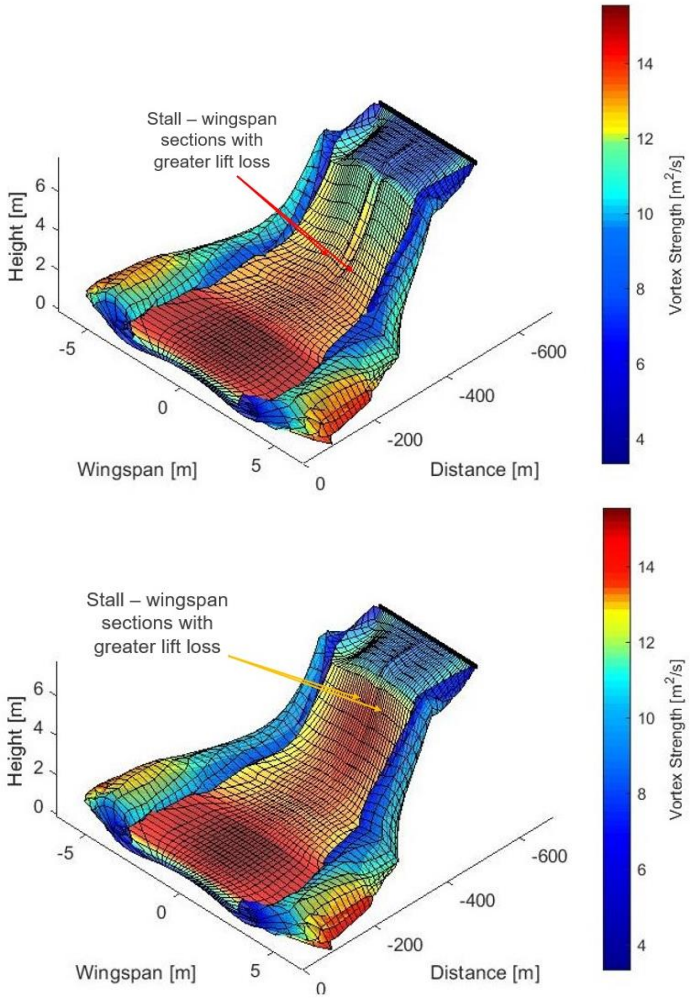

Fig. 7 Wakes generated by the wing in takeoff for α_o=12.0 deg and M_θ=3.0 (top) and α_o=12.0 deg and K_θ=2.5 (bottom)

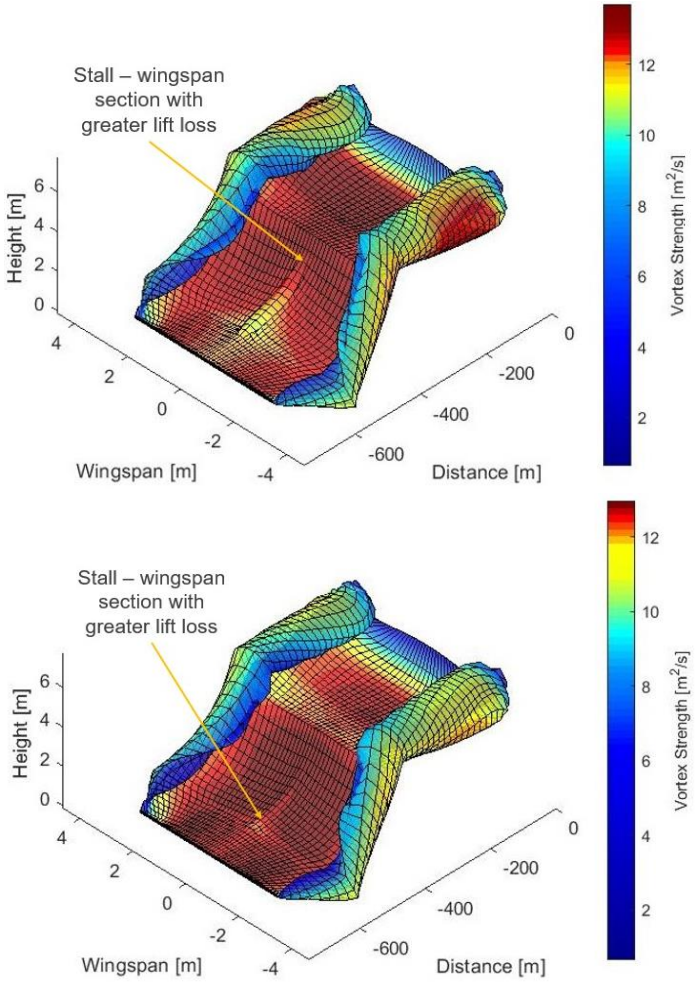

Fig. 8 Wakes generated by the wing in flare for α_o=11.0 deg and M_θ=1.5 (top) and α_o=10.0 deg and K_θ=1.5 (bottom)

Figs. 5 and 6 show the lift coefficient obtained for the wing in takeoff and flare, respectively, for different values of α_o and K_θ or M_θ. These values are compared with the maximum lift coefficient in static ground effect as functions of H/b. The lift coefficient achieved by the wing in stall for takeoff and flare maneuvers are shown in Tables 4 and 5, respectively, and it is seen that these are lower than those estimated at a fixed height above the ground. In unsteady flow, the aerodynamic forces and moments of an airplane or wing are linked not only to the values of the instantaneous variables, but also to their entire history (Hao *et al.* 2019). In dynamic ground effect, the aerodynamic coefficients are related to a specific history of the flightpath or trajectory because of flow downstream (Boschetti *et al.* 2020). When the wing changes its height as a function of time, the wing generates an induced angle of attack and a flow separation distribution different from those attained at the same height when the wing flies at a fixed height aboveground. Therefore, the aerodynamic characteristics achieved by the wing in stall in dynamic ground effectare different from those obtained in static ground effect.

Finally, Fig. 7 shows the wake generated in takeoff maneuvers for α_o=12.0 deg and M_θ=3.0, and α_o=12.0 deg and K_θ=2.5, in which the stall occurs at H/b=0.3878 and H/b=0.8624, respectively. Fig. 8 shows the wakes for flare maneuvers for α_o=11.0 deg and M_θ=1.5, and α_o=10.0 deg and K_θ=1.5, in which the wing goes to stall at H/b=0.7376 and H/b=0.1744, respectively. These wakes are shown to present their development during the mentioned maneuvers since the wake shape and its position with respect to the wing influences the components of the ***RHS*** vector and the effective angle of attack distribution along the wingspan at each time interval, thus influencing the aerodynamic history of the wing and the stall in dynamic ground effect. The wakes presented are developed for the entire maneuver even after the stall.

In Figs. 7 and 8, it is seen that the wingtip vortices are more developed at higher heights whereas near the ground these vortices are flattened and widened due to the ground plane. Additionally, differences in the wake wing root vicinity due to the vortex strength distribution for each specific maneuver can be appreciated. By comparing Figs. 7 and 8, it is observed that the shape of the wake on the wing root vicinity developed differently in take-off than in flare. During take-off, two peaks are produced outward from the wake wing root vicinity since the aerodynamic history generated lower values for the point of flow separation within semiwingspan sections 0.2 and 0.4, thus greater lift losses on the wing studied during the maneuver are encountered within these wingspan sections. During flare, a peak is produced on the wake on the wing root vicinity due to greater vortex strength corrections at these wingspan sections, hence greater lift losses occurred on wingspan sections on the wing root vicinity, similarly to the stall in static ground effect.

4. Conclusions

This work shows the evaluation of the stall behavior of a rectangular wing of R_A=8.587 in static and dynamic ground effect using a self-developed code based on the unsteady vortex-lattice method with a Kirchhoff-based correction. The code was validated against wind tunnel data from a wing in static ground effect. The maximum difference between the maximum lift coefficients estimated using the present code and the experimental data for $H/b \geq 0.116$ is 3.05 %.

The lift coefficient achieved by a straight wing in stall in takeoff and flare are lower than those estimated in static ground effect. At a fixed height aboveground, the wing reduces its maximum lift coefficient as the ground proximity increases. However, this behavior is different in dynamic ground effect due to the maneuver history dependence of the aerodynamic coefficients. Consequently, it can be concluded, based on the results obtained herein, that the stall behavior of a wing in dynamic ground effect depends on the history of the maneuver.

Acknowledgments

This research did not receive any specific grant from funding agencies in the public, commercial, or not-for-profit sectors.

References

Blakelock, J.H. (1991), *Automatic Control of Aircraft and Missiles*, John Wiley & Sons, Inc., New York, U.S.A.

Boeing. (2019), “Statistical summary of commercial jet airplane accidents worldwide operations 1959-

2018", Boeing Commercial Airplanes, Seattle, Washington, D.C., U.S.A.
Boschetti, P., Cárdenas, E., Amerio, A. and Arevalo, A. (2010), "Stability and performance of a light unmanned airplane in ground effect", *Proceedings of the 48th AIAA Aerospace Sciences Meeting Including the New Horizons Forum and Aerospace Exposition*, Orlando, Florida, U.S.A., January.
Boschetti, P.J., Cárdenas, E.M., González, P.J. and Merkl, A. (2020), "Nonlinear aerodynamic model for wings in dynamic ground effect", *J. Aircraft*, **57**(6), 1234-1241. https://doi.org/10.2514/1.C035853.
Boschetti, P.J., Quijada, G. and Cárdenas, E.M. (2016), "Dynamic ground effect on the aerodynamic coefficients of a wing using a panel method", *Proceedings of the AIAA Atmospheric Flight Mechanics Conference*, Washington, D.C., U.S.A., January.
Boschetti, P.J., Quijada, G.M. and Cárdenas, E.M. (2017), "Dynamic ground effect on the aerodynamic coefficients using a panel method", *J. Aircraft*, **54**(2), 838-844. https://doi.org/10.2514/1.C034098.
Chen, Y.S. and Schweikhard, W.G. (1985), "Dynamic ground effects on a two-dimensional flat plate", *J. Aircraft*, **22**(7), 638-640. https://doi.org/10.2514/3.45179.
Dias, J.N. (2016), "Nonlinear lifting-line algorithm for unsteady and post-stall conditions", *Proceedings of the 34th AIAA Applied Aerodynamics Conference*, Washington, D.C., U.S.A., January.
dos Santos, C.R., and Marques, F.D. (2018), "Lift prediction including stall, using vortex lattice method with Kirchhoff-based correction", *J. Aircraft*, **55**(2), 887-891. https://doi.org/10.2514/1.C034451.
Fischenberg, D. (1995), "Identification of an unsteady aerodynamic stall model from flight test data", *Proceedings of the 20th Atmospheric Flight Mechanics Conference*, Baltimore, Maryland, U.S.A., August.
Hao, D., Zhang, L., Yu, J. and Mao, D. (2019), "Modeling of unsteady aerodynamic characteristics at high angles of attack", *Proc. Inst. Mech. Eng. Part G J. Aerosp. Eng.*, **233**(6), 2291-2301. https://doi.org/10.1177/0954410018776527.
Katz, J. and Plotkin, A. (2001), *Low-Speed Aerodynamics*, Cambridge University Press, New York City, U.S.A.
Lee, T., Majeed, A., Siddiqui, B. and Tremblay-Dionne, V. (2018), "Impact of ground proximity on the aerodynamic properties of an unsteady airfoil", *Proc. Inst. Mech. Eng. Part G J. Aerosp. Eng.*, **232**(10), 1814-1830. https://doi.org/10.1177/0954410017703416
Leishman, J.G., and Beddoes, T.S. (1989), "A semi-empirical model for dynamic stall", *J. Amer. Helicopter Soc.*, **34**(3), 3-17. https://doi.org/10.4050/JAHS.34.3.3
Merkl, A., Boschetti, P.J. and Cardenas, E.M. (2019), "Dependence of the flight-path on the aerodynamic characteristics of rectangular wings due to dynamic ground effect", *Proceedings of the AIAA Scitech 2019 Forum*, San Diego, California, U.S.A., January.
Murua, J., Palacios, R. and Graham, J.M.R. (2012), "Applications of the unsteady vortex-lattice method in aircraft aeroelasticity and flight dynamics", *Prog. Aerosp. Sci.*, **55**, 46-72. https://doi.org/10.1016/j.paerosci.2012.06.001.
National Transportation Safety Board. (2012), "Crash during experimental test flight Gulfstream Aerospace Corporation GVI (G650) N652GD Roswell, New Mexico, April 2, 2011," Washington, D.C., U.S.A.
Nuhait, A.O. (1995), "Unsteady ground effects on aerodynamic coefficients of finite wings with camber", *J. Aircraft*, **32**(1), 186-192. https://doi.org/10.2514/3.46699.
Nuhait, A.O. and Mook, D.T. (1989), "Numerical simulation of wings in steady and unsteady ground effects", *J. Aircraft*, **26**(12), 1081-1089. https://doi.org/10.2514/3.45884.
Páez Castro, L.I. (2019), "Simulación del perfil aerodinámico NACA 4415 en vuelo libre y en efecto suelo", Engineering Final Project, Universidad Simón Bolívar, Caracas, Venezuela.
Quijada, G., and Boschetti, P.J. (2015), "Linear computational fluid dynamic analysis of dynamic ground effect of a wing in sink and flare maneuvers", *Proceedings of the AIAA Atmospheric Flight Mechanics Conference*, Kissimmee, Florida, U.S.A., January.
Rumsey, C.L. and Slotnick, J.P. (2015), "Overview and summary of the second AIAA high-lift prediction workshop", *J. Aircraft*, **52**(4), 1006-1025. https://doi.org/10.2514/1.C032864.
Rumsey, C.L., Slotnick, J.P. and Sclafani, A.J. (2019), "Overview and summary of the third AIAA high lift prediction workshop", *J. Aircraft*, **56**(2), 621-644. https://doi.org/10.2514/1.C034940.
Rumsey, C.L., Slotnick, J.P., Long, M., Stuever, R.A. and Wayman, T.R. (2011), "Summary of the first

AIAA CFD high-lift prediction workshop", *J. Aircraft*, **48**(6), 2068-2079. https://doi.org/10.2514/1.C031447.

Sarpkaya, T. (1989), "Computational methods with vortices-The 1988 Freeman scholar lecture", *J. Fluid. Eng.*, **111**(1), 5-52. https://doi.org/10.1115/1.3243601.

Staufenbiel, R.W. and Schlichting, U.J. (1988), "Stability of airplanes in ground effect", *J. Aircraft*, **25**(4), 289-294. https://doi.org/10.2514/3.45562.

Syms, G.F. (2002), "Low-order method for predicting aerodynamic performance degradation due to ground icing", *J. Aircraft*, **39**(1), 59-64. https://doi.org/10.2514/2.2895.

Traub, L.W. (2015), "Experimental and analytic investigation of ground effect", *J. Aircraft*, **52**(1), 235-243. https://doi.org/10.2514/1.C032676.

AP